Nano Today (2016) 11, 212—227

Available online at www.sciencedirect.com

ScienceDirect

journal homepage: www.elsevier.com/locate/nanotoday

REVIEW

Principles of nanoparticle formation by flash nanoprecipitation

Walid S. Saad[a], Robert K. Prud'homme[b,*]

[a] *Department of Chemical and Petroleum Engineering, American University of Beirut, Beirut 1107 2020, Lebanon*
[b] *Chemical and Biological Engineering, Princeton University, Princeton, NJ 08544, USA*

Received 4 December 2015; received in revised form 24 March 2016; accepted 4 April 2016
Available online 3 May 2016

KEYWORDS
Flash nanoprecipitation;
Nanoparticle;
Supersaturation;
Block copolymer;
Drug delivery

Summary Rapid precipitation is an efficient approach for engineering materials at the nanoscale. By controlling solute nucleation and growth rates in solvent precipitation processes, the size of the resulting nanoparticles (NP) can be controlled. This review discusses Flash Nanoprecipitation (FNP), a technique developed for NP formation using copolymer stabilization. FNP has been explored for various applications, including NP formulation for drugs and imaging agents. The review highlights mixing considerations, supersaturation requirements, and stabilizer selection to provide controlled size NP *via* FNP, and includes a summary of current understanding of the FNP process, as well as relevant examples and applications.

The utility of nanoparticles from hydrophobic constructs

The recently acquired ability to engineer materials at the nano-scale in order to achieve desired properties at the macro-scale has made nanotechnology of interest in several fields. In particular, nanoparticles (NP) are being explored as novel tools for applications including solar energy conversion and photovoltaics [1], pigments and catalysts [2], and perhaps most actively, medicine [3,4]. In nanomedicine, formulating therapeutic components that are often hydrophobic in nature into the nanoparticle size range of a few nm to about 100 nm provides several advantages, including: (1) solubilize hydrophobic drugs, (2) increase bioavailability and total absorption of orally administered drugs [5], (3) concentrate cancer drugs at the tumor site by passive targeting through the Enhanced Permeability and Retention (EPR) effect, and active targeting through ligand—receptor interactions [6], (4) deliver drugs to the lungs [7], and (5) modify the drug activity through NP surface modification, for instance using polyethylene glycol (PEG), which reduces complement binding and decreases the drug clearance rates during *in vivo* circulation [8]. Research efforts in that area lead several nanomedicine-based therapies to reach the market [9].

* Corresponding author at: Department of Chemical Engineering, Princeton University, Princeton, NJ 08544, USA.
Tel.: +1 609 258 4577; fax: +1 609 258 0211.
E-mail address: prudhomm@princeton.edu (R.K. Prud'homme).

http://dx.doi.org/10.1016/j.nantod.2016.04.006
1748-0132/

NP formation by rapid precipitation affords high drug loading contents through the coating of NP surface using protecting agents. The coating materials are of amphiphilic nature, and include block copolymers and lipids. These provide steric stabilization and limit instabilities due to aggregation and Ostwald ripening [10]. In contrast, polymeric drug micelles formed by imbibing drugs into the hydrophobic core of a micelle are fundamentally different and are thermodynamically bound to lower drug loading contents than NP [11].

The synthesis route used for NP formation determines the resulting NP properties. Several factors require consideration to afford stable, controlled-size distribution of high loading NP of hydrophobic constructs. This can be achieved through imposing rapid processing conditions that yield short length scales where nucleation, growth, and the subsequent equilibration of NP are controlled [12]. In rapid precipitation, the nucleation and growth time of a hydrophobic molecule under supersaturated conditions is matched with the aggregation time of the stabilizing amphiphilic molecule, resulting in narrow, controlled size distribution of NP.

This review summarizes factors controlling NP formation by block copolymer directed, rapid precipitations.

Overview of particle size from rapid precipitations

Precipitation is a commonly used technique in the pharmaceutical industry. Active pharmaceutical ingredients (API) are often precipitated from solution through the addition of a non-solvent, or through temperature quenching. Controlled precipitation conditions are used to optimize the API particle size, which affects drug product performance requirements such as dissolution properties and bioavailability [13]. NP formation by temperature quenching remains challenging due to low supersaturation levels and non-uniform spatial temperature distribution in the precipitation vessel, resulting in wide particle size distributions.

In rapid precipitation, mixing conditions control the final particle size distribution. Mixing characteristic time can be categorized as macromixing (decimeter scale, *e.g.* on the order of the vessel), mesomixing (millimeters, on the order of the turbulent eddies that form when viscous forces dominate over inertial ones), or micromixing (micrometer scale, on the order of molecular diffusion in fluid lamellae) [14,15]. Micromixing conditions are required to afford characteristic times on the order of nucleation and growth times needed for the formation of NP with controlled size distributions.

Nucleation is a strong function of supersaturation

Starting from a single phase of molecularly dissolved molecular species in solution, rapid precipitation is achieved through imposing a condition of high supersaturation. This leads to nucleation and growth of particles at a nucleation rate J given by [16]

$$J = A \exp\left(\frac{-16\pi\gamma^3 v^2}{3k^3T^3(\ln(S))^2}\right) \quad (1)$$

Where A is a constant, γ is the surface tension, ν is the molar volume, k is Boltzmann's constant, T absolute temperature, and S the supersaturation. The relationship reveals the strong dependence of nucleation on both supersaturation and temperature.

Starting from the supersaturated state, nuclei start to form once the critical nucleation concentration is reached. As a result, the bulk solute concentration decreases. The concentration drop freezes any additional nuclei formation and leads to the growth of the already formed nuclei by aggregation and association with solute molecules in the bulk. The growth continues until the solute concentration reaches the equilibrium saturation concentration.

From the processing aspect, creating homogenous nucleation conditions are challenging, particularly because achieving high local supersaturation levels is technically difficult. For instance, particle creation by solvent/anti-solvent mixing in a batch vessel does not provide the micromixing conditions needed for high local supersaturations. This results in wide particle size distributions and subsequent solute precipitation. Mahajan and Kirwan [17] overcame the mixing limitation by using a grid mixer device with a characteristic mixing time of <3 ms to study the nucleation and growth kinetics of pharmaceuticals. The short micromixing time provides rapid and uniform solute mixing, which allows for the nucleation rates to be controlled. The authors investigated the precipitation of lovastatin and asparagine monohydrate over low to moderate supersaturation ranges. Their results reveal an increase in supersaturation levels for both drugs is accompanied by an increase in the nucleation rates as predicted by Eq. (1), and a decrease in the growth rates [16,17]. Therefore, in order to afford NP smaller than a few hundred nanometers, nucleation should be favored over growth. High nucleation rates provide high nuclei density resulting in high nanoparticle yield. When growth is favored over nucleation, few nuclei form and will likely grow to micron-size particles.

Particle formation can also occur through a spinodal decomposition mechanism. Starting with an unstable state under very high supersaturation conditions, phase separation occurs spontaneously to produce a solute-rich phase. [14]

Controlling growth rates

Key diffusion limited processes for mass transport involved in particle growth include [12]:

a. Diffusion-limited stepwise molecular growth of solute on the particle surface
b. Particle aggregation determined by the Smoluchowski kinetics with no barrier to aggregation
c. Ostwald ripening by diffusion mass transfer

Calculated maximum growth rates and the corresponding dependence on particle diameter for β-carotene obtained for each process [12] are illustrated in Fig. 1. These processes affect NP due to their small size and the strong dependence of growth rate G (nm/min) on particle diameter, d (nm), represented as n ($G \sim 1/d^n$), on the secondary axis of the graph. The fast rates shown in the

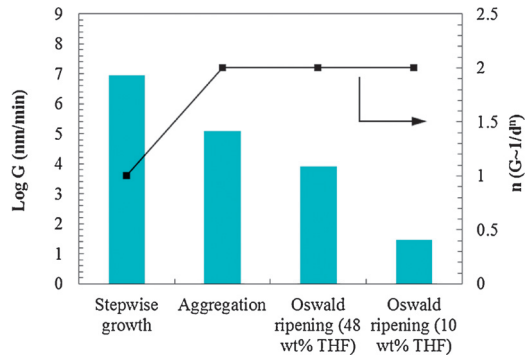

Figure 1 Estimated diffusion-limited processes growth rates *G* (nm/min) for β-carotene. The secondary axis shows the dependence of growth rate on particle size. Lines connecting data points are added for clarity [12].

figure, particularly through stepwise growth and aggregation (Smoluchowski kinetics) lead to fewer particles and larger particle sizes over time. Strategies are put in place to favor nucleation over growth and limit processes leading to larger particles and low NP yield.

Aggregation can be limited in the case of surface charge formation due to the chemical nature of the solute. Alternatively, surface stabilizers such as amphiphilic block copolymers provide steric stabilization and prevent particle aggregation. Fig. 1 also shows that Ostwald ripening rates can be drastically reduced by changing the solvent quality for the solute, *i.e.* reducing the solute bulk solubility. These results have been confirmed both experimentally and through numerical simulations based on the Lifshitz—Slyozov—Wagner (LSW) theory [10,18].

The next section provides an overview of flash nanoprecipitation (FNP), a recently established technology that controls the process thermodynamic and kinetic conditions to promote nucleation over growth of particles, yielding stable, controlled-size NP.

Overview of Flash Nanoprecipitation (FNP)

The FNP process provides the local supersaturation needed for particle nucleation by fast mixing of a stream containing a molecularly dissolved solute and stabilizing molecule with an opposing stream containing a miscible solvent, which acts as a non-solvent for the solute and stabilizer. Mixing occurs in the turbulent regime in a confined volume, affording high-energy dissipation rates, and providing the supersaturation conditions required for simultaneous precipitation of the solute and stabilizer. The block copolymer inhibits further growth of the solute particles, and provides steric stabilization through the hydrophilic block on the surface of the particle. The work of Johnson and Prud'homme revealed a characteristic mixing time in this process on the order of milliseconds [15]. This represents a key feature of FNP and distinguishes it from the alternate solute NP/micelle formation technologies such as emulsification and diffusion, since it allows for diffusion limited growth of particles that prevail under high supersaturation conditions. In contrast, emulsification and dialysis-based techniques involve precipitation of the drug followed by block copolymer stabilization, which results in poor drug encapsulation efficiencies and loading contents.

The supersaturation condition

Rapid mixing, on the order of milliseconds, is required to affect homogenous conditions for the creation of uniform local high supersaturation. This leads to precipitation of any solute or molecule existing above its saturation level, irrespective of its chemical nature. As a result, rapid precipitation using solvent addition, including FNP, is a versatile approach for solute particle formation, particularly in the pharmaceutical industry where over 40% of new chemical entities under development are poorly water soluble [19].

Since imposing a condition of high supersaturation is sufficient for particle creation, multiple species can be co-precipitated using FNP. Depending on the application of interest, combinations of drugs, imaging agents, or other solutes of interest can be easily formulated into the particle core. Some examples are discussed in subsequent sections.

Stabilization using amphiphilic block copolymers

Molecularly dissolved amphiphilic block copolymers which contain hydrophilic and hydrophobic blocks self-assemble when the solvent quality for one block is decreased. This feature renders them useful as surface stabilizers for nascent particles and help control the particle size distribution by adsorbing on the particle surface and preventing particle aggregation. The self-assembly of surfactants and amphiphilic polymers is driven by supersaturation. In the context of FNP, the solvent quality jump imposed by rapid mixing leads to precipitation of the organic solute and adsorption of the hydrophobic block of the copolymer on the particle surface through hydrophobic interactions. Further growth of the solute particles is inhibited through the steric stabilization provided by the polymer's hydrophilic block.

The effect of polymer stabilization in FNP is illustrated in Fig. 2. In this example, vitamin E succinate (VES) particles produced without any stabilizing polymer using FNP result in a larger initial particle size and subsequent aggregation than VES particles made using methoxy poly(ethylene glycol)-*b*-poly(ε-caprolactone) (PCL-*b*-PEG) as a stabilizer. The block copolymer interferes with the nucleation and growth kinetics of the solute particles and arrests particle growth. The end result is smaller particle size and a narrower particle size distribution (Fig. 2). The block copolymer provides particle stabilization over prolonged periods, allowing for post processing of the NP and maintaining the original particle size distribution. Similar results have been demonstrated with β-carotene [20].

Block copolymer NP form kinetically frozen structures

The final state of block copolymer NPs formed *via* FNP is non-equilibrium, kinetically frozen. A study by Dormidontova provides insight into the kinetics of formation of block copolymer NP from a unimer solution [21]. The study

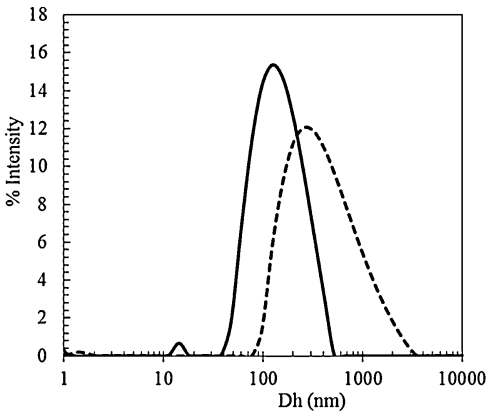

Figure 2 Initial intensity-weighed particle size distribution for VES particles (dashed line) produced *via* FNP as determined by dynamic light scattering. The aggregation is limited when a stabilizing polymer is used (PCL-*b*-PEG, solid line) with VES at weight ratio of 1/1. The result is a smaller average particle size and a narrower particle size distribution than VES precipitated *via* FNP without any stabilizers, which yields visible aggregates shortly after particle formation.

uses a scaling model with Kramer's theory to obtain association/dissociation rate constants for micelle formation *via* the unimer exchange and micelle fusion/fission mechanism. The results show micelle fusion/fission dominates at early stages of micelle formation, while unimer exchange becomes active at longer times to bring the micelle to the equilibrium size. Ligoure and Leibler [22] identify two regimes in polymer chain grafting to a flat plate. A fast regime dominated by diffusion of polymer chains in solution until an overlapping brush is formed, and a slower regime involving polymer moving across the soluble brushes, a slow process leading to equilibrium.

In FNP, the fast mixing provides high initial supersaturation conditions for the block copolymer. Following fusion up to a critical size, that of overlapping coronas, the subsequent unimer exchange process that normally brings these structures to dynamic equilibrium micelles is inhibited due to the high energy cost associated with the polymer chain diffusion under high supersaturation conditions. As a result, the formed NP are kinetically frozen [23].

The following sections address aspects of mixing, supersaturation, and polymer stabilization individually.

Mixing considerations

The starting point for NP formation by rapid precipitation is mixing. In this section, the nature of turbulent mixing, and the experimental and theoretical characterization of mixing in the FNP process are discussed.

Nature of turbulent mixing

Since particle nucleation and growth events occur at the molecular level, mixing at the same level, *i.e.* micromixing is needed to control the process kinetics. In confined mixing geometries such as CIJ and MIVM, a high turbulent energy dissipation region is produced, which enhances the fluid mixing rates and provides the proper mixing scale for controlled nucleation and growth [15,16]. Micromixing under turbulent conditions involves engulfment, where two liquid compartments surround each other to form increasingly thinner lamellae, and deform through elongation and shear. The resulting laminated structures allow for molecular exchange by diffusion [24,25].

The corresponding time scale for molecular diffusion τ_G is given by [26]:

$$\tau_G = \tau_E \left(0.030 + \frac{17,050}{Sc}\right)^{-1} \quad (2)$$

Where *Sc* is the Schmidt number and τ_E the engulfment time constant, which describes the viscous convective deformation of the fluid elements:

$$\tau_E = 17.24 \left(\frac{\vartheta}{\varepsilon}\right)^{1/2} \quad (3)$$

Where ϑ is the kinematic viscosity (m^2/s) and ε the energy dissipation rate (J/kg s).

Controlling the mixing timescale is critical in the NP formation process, since the mixing time has to match the characteristic nucleation and growth time of NP. As a result, mixing characterization becomes the first step into designing NP production technologies.

Geometries: CIJ, MIVM

In FNP, mixing of the organic solute and stabilizing polymer with the anti-solvent occurs in a confined mixing chamber. The chamber geometry and size can vary [15].

In CIJ mixers, two streams collide against each other in a cavity. The CIJ mixer geometry, however, limits the ratio of solvent/non-solvent that can be used in the mixing process since the opposing jets need to collide at equal momentum in the mixing chamber. This prevents higher supersaturation levels from being achieved through increasing the non-solvent/solvent ratios, and restricts the use of the technology to the class of hydrophobic solutes with very poor water solubility. In order to overcome this limitation, a multiple inlet vortex mixer (MIVM) design, which allows for unequal solvent/non-solvent ratio mixing, is used for mixing conditions requiring flexibility in the inlet streams content and flow rate ratios. Such a configuration is practical for reactive systems or for mixing streams with immiscible components. Alternatively, a hand operated CIJ mixer that does not require pumps for operation was developed in the Macosko lab [27]. In this setup, the two streams are introduced into the CIJ mixer inlets through handheld syringes, and the outlet stream further diluted in a solution of the anti-solvent (water) to quench aggregation and enhance the NP stability. The mixer is inexpensive to produce and requires less volume to operate than the pump-controlled CIJ mixer.

The CIJ, two-jet MIVM, and four-jet MIVM geometries used in FNP are shown in Fig. 3. The sole requirement in the FNP process is the creation of turbulent mixing conditions in a confined volume. Hence, other mixer designs may be considered provided they lead to turbulent mixing conditions.

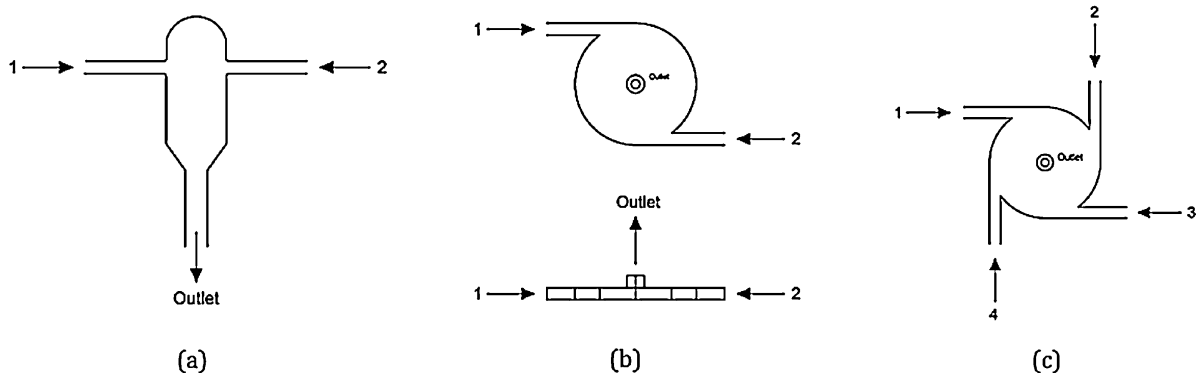

Figure 3 Various mixer geometries are used to produce conditions of turbulence with high energy dissipation rates in a confined volume: (a) CIJ mixer, (b) two-inlet MIVM top and side views, and (c) four-inlet MIVM.

Characterization using competitive reactions

In the precipitation of organic actives by crystallization, micromixing affects the final crystal size distribution [28]. Johnson and Prud'homme characterized micromixing effects in CIJ mixers used for the production of sub-micron particles of organic solutes [15].

The experimental approach used for evaluating micromixing efficiency in opposed jets reactors involves running competitive reactions in series or in parallel [29]. In such experiments, reactions yielding few, easily analyzed products, with well characterized kinetics and good reproducibility are selected [29]. Generally, these reactions are of the type

$$A + B \xrightarrow{k_1} P_1 \quad (4)$$

$$D + B \xrightarrow{k_2} P_2 \quad (5)$$

Where A, B, D, are chemical reactants, P_1, P_2 reactions products, and k_1 and k_2 are chemical reaction kinetic constants [15]. In these parallel reaction systems, $k_1 \gg k_2$. Efficient mixing renders the first reaction instantaneous and favors formation of P_1, while P_2 formation is not detected. Therefore, monitoring P_1, P_2 formation provides an indication of mixing efficiency. Johnson and Prud'homme used the hydrochloric acid/sodium hydroxide neutralization reaction (fast) competing with the acid catalyzed hydrolysis of 2,2-dimethoxypropane (DMP, slow) to characterize micromixing in CIJ mixers [15]. They used the Damköhler number (*Da*) to gauge mixer performance. Their study reveals the reaction selectivity was proportional to *Da*, and provides scale-up criteria for CIJ mixers.

Simulations with computational fluid dynamics

CIJ and MIVM mixers have been characterized using computational fluid dynamics (CFD) studies. In some cases, CFD is complemented with experimental measurements aiming at characterizing flow behavior. For instance, mixing in an MIVM mixer was characterized in the laminar and turbulent regimes using microscopic particle image velocimetry [30,31].

Fox et al. developed a CFD model for the prediction of reactive micromixing under turbulent conditions, and validated their results with experimental data for both CIJ [32] and MIVM [33] mixer geometries. The model uses the direct quadrature method of moments coupled with the interaction by exchange with the mean (DQMOM-IEM) to solve the composition probability density function transport equation. CFD results for DMP conversion *vs.* Reynolds number (*Re*) in parallel competitive reactions were in good agreement with experimental data with no adjustable parameters. In the case of MIVM geometry, mixing was characterized under various inlet configurations and demonstrates homogeneous mixing conditions for mixing at $Re > 1600$ [33]. In separate studies, CFD predictions for mixing and reaction in CIJ mixers correlated well with experimental data at various jet *Re* values, for different mixer geometries and reactant concentrations [34,35]. The energy dissipation profiles within the mixers were identified. The studies provide a reliable CFD model for aiding in the design and scale up of CIJ and MIVM mixers.

Significant advances have been achieved in CFD prediction of polymer-based nanoparticle formation through the work of Di Pasquale et al. [36,37], who modeled nanoparticle formation using DQMOM-IEM. Their initial results for poly(ε-caproloactone) (PCL) show good agreement between simulation and experimental data when the polymer molecular volume was used as a fitting parameter for each solvent/non-solvent ratio used in the precipitation process [36]. The model relies on the classical nucleation theory developed for small solute molecules, for which most parameters are known, including the diffusion coefficient, diameter, and molecular volume [37]. In the case of polymer precipitation, the parameters change with changing solvent compositions and are difficult to determine. Di Pasquale et al. improved on the previous model by introducing an augmented nucleation theory model [37], resulting in a better fit with experimental data without the need for parameter fitting.

Supersaturation considerations

FNP is centered on exploiting high supersaturation conditions to induce nucleation and growth of solute particles under controlled solvent/non-solvent mixing conditions. In the case of therapeutic compounds, several approaches can

be used to increase supersaturation levels and optimize the conditions for NP formation.

Determining hydrophobicity

Determining the solubility profile of solutes of interest under various solvent/non-solvent ratios aids in determining the optimal conditions for imposing high supersaturation conditions needed for controlled particle growth. For hydrophobic solutes, a low ratio of organic solvent/water results in high supersaturation levels and favors NP formation by FNP. A high organic solvent content enhances the hydrophobic solute solubility in the solvent mixture and results in lower supersaturation ratios, which limits the effectiveness of FNP at producing controlled size NP.

A commonly used indicator for drug hydrophobicity is the octanol/water partition coefficient, Log P, which can be used to estimate drug solubility *via* the semi-empirical relationship [38]

$$\text{Log}\, S = 0.5 - \text{Log}\, P - 0.01(T_m - 25) \quad (6)$$

Where S is the solute molar concentration in a saturated aqueous solution in equilibrium with the most stable solute crystalline form, and T_m is the solute melting temperature (°C). A higher Log P value indicates higher hydrophobicity and lower water solubility, which results in higher NP solute loadings. Therefore, Log P values are used as an indicator of the tendency of solutes to partition into the core of NP rather than dissolve in the surrounding aqueous environment [39]. Log P values are obtained experimentally, computationally, or through semi-empirical methods [40].

Mixed solvents and solvent selection

Supersaturation levels can be modified through changing the solute concentration or the solute solubility in the mixed solvent, both of which can be controlled in FNP. The solute concentration can be increased in the pre-mixed solvent stream through selecting water-miscible solvents affording high solute solubility. The solute solubility is modified through changing the mixed solvent quality. Using the MIVM mixer geometry, the solvent/water ratio can be changed by changing the individual stream flow rate, providing a wide range of solute solubility in the mixed product, and resulting in different values of supersaturation. As a result, both the choice of solvent and the water/solvent ratio used during mixing can be used to affect solute supersaturation levels. Higher supersaturation levels are achieved through increasing water/solvent ratios to reduce the solute solubility in the final solution, up to a maximum beyond which solute dilution reduces the supersaturation level [16].

Representative examples of solvents used in FNP are listed in Table 1. The table also includes the solvent boiling point, which is used to determine the most efficient solvent removal technique. High boiling point solvents such as dimethyl sulfoxide (DMSO) are best removed by dialysis, while low boiling point solvents such as tetrahydrofuran (THF) can be removed by vacuum evaporation.

Supersaturation and solids concentrations affect final particle size

Particle size in FNP can be modified through changing supersaturation levels, solute concentrations, or the addition of co-precipitates that alter the nucleation process, resulting in a different particle size.

Supersaturation levels can be changed easily in FNP. The MIVM mixer geometry can be used to vary the ratio of organic solvent/non-solvent (water) mixing streams. Supersaturation affects nucleation rates by means of Eq. (1), which in turn affects the resulting particle size distributions. Higher supersaturation levels leads to a higher number of nucleating sites, resulting in smaller NP. While NP size control *via* nucleation involving amphiphilic block copolymers is not fully understood, two mechanisms are proposed to explain the shift in particle size distribution following a change in supersaturation [49]. In one case, the high solute supersaturation levels induce homogeneous nucleation and growth which is arrested by polymer assembly on particle surface. Alternatively, hydrophobic domains on the block copolymers serve as nucleating sites for solute molecules to nucleate heterogeneously. Particle dilution and steric hindrance of the hydrophilic block of the copolymer lead to a halt in particle growth. In one application, β-carotene supersaturation was modified using an MIVM mixer by changing the solvent (THF) to non-solvent (water) streams ratio from 1/20 (THF/water, vol%) to 1/4. The corresponding NP size was changed from about 70 nm at 1/20 (THF/water) to about 120 nm at 1/4 (THF/water) as a result of decreasing supersaturation through decreasing the water fraction [10].

NP size can also be modified by changing the solute concentration. As solute concentration increases, its corresponding nucleation and growth rates increase faster than

Table 1 Representative examples of solvents used in FNP.

Solvent	Boiling point [41]	Removal technique	Reference
THF	65 °C	Vacuum evaporation	[42]
THF	65 °C	Dialysis	[43,44]
Cyclopentanone	130.57 °C	Spray drying	[45]
Ethanol	78.29 °C	Dialysis or ultrafiltration	[46]
Dimethylformamide (DMF)	153 °C	Dialysis	[47]
Dimethyl sulfoxide (DMSO)	189 °C	Dialysis	[47]
1-Methyl-2-pyrrolidone (NMP)	202 °C	Dialysis	[47]
Methanol	64.6 °C	Dialysis	[48]

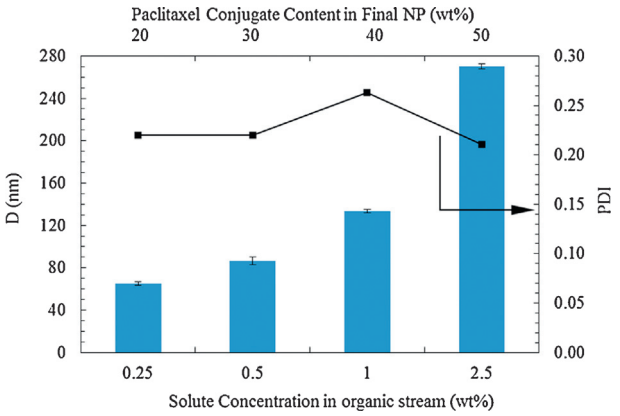

Figure 4 Effect of active concentration on particle size prepared by FNP. Increasing the solute initial concentration leads to an increase in particle size. Data shown for paclitaxel-VES conjugate/VES mixed with PCL-*b*-PEG in THF using the MIVM mixer. Lines connecting PDI data points are added for clarity. The secondary (top) horizontal axis highlights the drug conjugate content in the final NP.

the polymer aggregation rate, providing additional time for particle growth before polymer stabilization, and resulting in larger particle size. Fig. 4 demonstrates control of particle size by changing solute concentration for paclitaxel-VES conjugate/VES mixture (1/1 weight ratio) stabilized with 0.5 wt% PCL-*b*-PEG (7000-*b*-5000 g/mol, respectively). NP size was varied by changing the starting solute concentration in THF, while the stabilizing polymer concentration was kept constant.

Alternatively, particle size can be modified using hydrophobic solutes that act as seeding agents promoting particle growth. In one application, PCL homopolymer was co-precipitated with paclitaxel to produce NP with controlled particle size under fixed mass concentrations of paclitaxel and PCL. The number of nucleating sites that controls the number of growing paclitaxel particles was modified by changing the PCL molecular weight. Higher PCL molecular weight means fewer nuclei are available for subsequent drug growth, resulting in larger particle sizes. This effect is shown in Fig. 5 for paclitaxel NP formulated

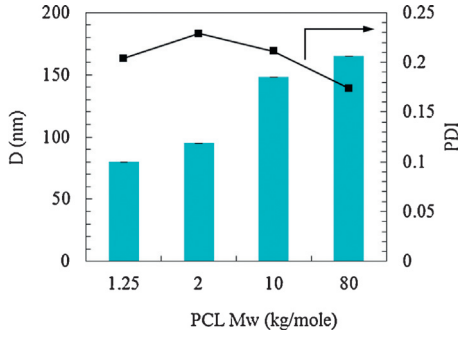

Figure 5 Effect of PCL homopolymer molecular weight on particle size prepared by FNP. Particle size is represented by bars and the corresponding PDI by filled squares. Lines connecting PDI data points are added for clarity. This approach allows for particle size to be controlled independently of the active concentration.

using PCL homopolymer with molecular weight ranging from 1250 g/mol to 80,000 g/mol, and stabilized with PCL-*b*-PEG (2900-*b*-5000 g/mol, respectively). This technique has the advantage of controlling NP size independently of the active concentration.

Creating insoluble species

The supersaturation requirement in FNP makes the solute's low aqueous solubility a key requirement for its successful incorporation into NP. For solutes where supersaturation levels are low, several routes can be used to modify hydrophobicity, including conjugation, ion pairing, and complex formation.

In solute conjugation, the solute of interest is first conjugated to a hydrophobic species anchor, and then formulated into NP using FNP. This method aims at modifying the solute solubility through covalent attachment of to a hydrophobic molecule, such as a hydrophobic polymer or vitamin to form a drug conjugate exhibiting lower water solubility than the original active drug. The resulting increase in hydrophobicity is due to the hydrophobic nature of the anchor and the increased molecular weight of the resulting solute. Using this approach, hydrophilic solutes are rendered hydrophobic through conjugation to a hydrophobic anchor, and formulated into NP *via* FNP. The linker chemistry involved in the anchor-drug forming the conjugate controls the drug release rate. In one application, the nature of the linker chemistry and the hydrophobicity of the anchor were modified in paclitaxel conjugate NP prepared *via* FNP, resulting in extended circulation times and improved therapeutic efficacy *in vivo* compared with unmodified drug [50]. Hoye et al. proposed novel silicate ester prodrugs of paclitaxel and docetaxel, and determined the corresponding hydrolysis rates and cytotoxicity, providing a novel platform for modulating the drug release rate in drug conjugate NP [51]. The concept of conjugation to enhance supersaturation also applies to inorganic agents with applications to chemotherapy and *in vivo* imaging [16].

Alternatively, hydrophobicity can be increased through ion pair formation. Modification of weakly hydrophobic, ionizable API through ion pair formation results in salts with sufficient hydrophobicity to form stable NP *via* FNP. The solubility and crystallinity of cinnarizine, clozapine, and α-lipoic acid were modified *in situ* through pairing with salt forming agents during the FNP process to yield stable, controlled size NP [52]. The encapsulation efficiency and drug loading were controlled through the base-to-acid ratio in the organic stream. Unlike drug conjugation, the resulting formulation modifies API properties through ionic interactions, thus avoiding the need for FDA approval as a new chemical entity. Ion pairing expands the range of solutes which can be formulated into NP *via* FNP, to include weakly hydrophobic, ionizable molecules.

A similar approach has been used to precipitate siRNA and elucidate the mechanism of macromolecular structure formation during particle assembly [46,53]. In this approach, siRNA precipitation is induced through rapid mixing of a lipids solution dissolved in ethanol with an acidic aqueous solution of siRNA at a predetermined molar ratio of the ionizable lipid amine to siRNA phosphate (N/P). High

encapsulation efficiency can be obtained at low N/P through appropriate buffer species selection. Particle formation was followed by an annealing step in the 50% ethanol solution resulting from the mixing process. The annealing step enables the initially disorganized macromolecular structure to rearrange into ordered lamellar structures in the final product. Instability caused by Ostwald ripening was significantly inhibited through the use of structurally matched co-lipids and the modulation of lipid nanoparticle size [54].

The creation of insoluble species can also be achieved through pH change. In one study, Peptide B, a nine residue analog of an agonist for Bombesin Receptor Subtype 3, was precipitated into NP *via* FNP through organic/water solvent exchange and by a rapid pH switch from a value of three to a value of seven in aqueous media [47]. The study includes qualitative Brownian dynamics simulations that confirm the experimentally observed dependence of nanoparticle size on supersaturation.

Polymer stabilizers selection

This section provides an overview of the amphiphilic diblock copolymer selection and the corresponding properties affecting NP production by FNP.

Why use amphiphilic diblock copolymers?

Aqueous suspensions of hydrophobic solute NP are non-equilibrium systems. As evident from the discussion above, the high interfacial surface area resulting from reduced particle size renders such systems prone to aggregation, unless the surface is charged, or modified through adsorption of ionic surfactants or polymers. Highly charged surfaces yield flocculation at high salt concentrations, and increased protein binding, which limits their efficacy *in vivo* [55].

The use of amphiphilic diblock copolymers for NP stabilization offers several advantages in formulation processing and *in vivo* efficacy. Using PEG as the hydrophilic block leads to prolonged circulation times [55]. Diblock copolymers exhibit lower critical micelle concentration (cmc) than surfactants, which reduces the partitioning of the hydrophobic segment off of the NP surface *in vitro* and *in vivo*, resulting in enhanced stability and longer protection from opsonization *in vivo*. During NP formation by FNP, amphiphilic diblock copolymers arrest solute particle growth and provide stabilization before aggregation to the micron size occurs. Unlike graft and triblock copolymers, aggregation through bridging does not occur.

Block copolymer selection

The nature of the polymer used plays an important role in controlling the stability of NP produced by FNP. One study by Pustulka et al. investigated the structure and stability of β-carotene NP prepared by FNP using four different amphiphilic diblock copolymers, with a hydrophobic block M_w of about 10,000 g/mol, and a PEG M_w of 5000 g/mol as the hydrophilic block [56,57]. The hydrophobic blocks consisted of polystyrene (PS), PCL, polylactide (PLA), or poly(lactic-*co*-glycolic acid) (PLGA). For optimal stability, the results suggest the hydrophobic block of the diblock copolymer should be amorphous, possess a glass transition temperature (T_g) higher than the usage temperature, and have a large difference in its solubility parameter compared with PEG. The last requirement minimizes the risk of PEG chains partitioning into the NP core instead of providing surface protection, which reduces stability. Based on the results and the literature [58] PLGA-*b*-PEG provided the most suitable stability profile among the polymers tested due to its high T_g, biocompatibility, biodegradability, and amorphous state.

Kumar et al. evaluated the effect of the stabilizing polymer type used in NP of itraconazole and odanacatib prepared by FNP [59]. Two stabilizing polymers were used in the study: a diblock copolymer of PS-*b*-PEO (PS M_w 1000 g/mol, PEO M_w 3000 g/mol), and poloxamer P407, a block copolymer of polypropylene oxide and PEG. Both polymers have similar solubility parameters, leading to similar attachment energies on the NP surface. The resulting initial particle sizes produced by FNP were similar for both polymers. However, the state of the hydrophobic blocks differs under the experimental temperature conditions (5 °C and room temperature), where PS is a glassy structure (T_g = 95 °C), while P407 exists in a liquid state (T_g = −75 °C). As a consequence, P407 is kinetically active, capable of desorbing from the NP surface along with solute molecules, leading to increased solubilization of the drug. The end result is increased Ostwald ripening rates due to the increased drug effective bulk concentration. In contrast, the PS-*b*-PEO is better anchored on the NP surface due to the frozen state of PS, making the block copolymer less prone to desorption, and resulting in a more stable NP formulation, as shown by the experimental results.

Block copolymer concentration

The amount of stabilizer affects particle size until a critical size corresponding to $Da = 1$ is reached. In the region of turbulent mixing ($Da < 1$), particle size is not significantly affected by the stabilizing polymer concentration [60]. The effect of polymer concentration on average particle size for NP formed under turbulent mixing conditions is shown in Fig. 6. The polymer concentration has a minor effect on

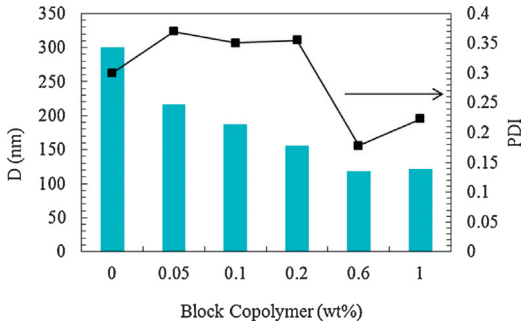

Figure 6 Particle size (bar) as a function of stabilizing PCL-*b*-PEG (3000-*b*-5000 g/mol, respectively) concentration at fixed VES concentration (1 wt%). Concentrations are based on the THF stream prior to mixing. Lines connecting PDI data points are added for clarity.

particle size beyond a critical amount needed for particle stabilization.

In one study, P407 was used to stabilize itraconazole NP under various mixing conditions [61]. Particle stabilization was tested through antisolvent precipitation with P407 stabilizer in the organic phase or in the aqueous phase, at concentrations below the cmc. When mixing with P407 in the aqueous phase, the polymer chains have to diffuse through the bulk aqueous phase and the aqueous/organic interface before providing drug stabilization, leading to insufficient surface coverage and particle growth by condensation and coagulation. The end result is larger particle sizes (600 nm at the lowest stabilizer concentration). Particle size decreased with increasing stabilizer concentration up to the region of $Da < 1$. Mixing with the stabilizer in the organic phase resulted in smaller particle sizes (290 nm under the same conditions) due to faster diffusion of the stabilizing polymer to the precipitating drug molecules.

Surface coverage on NP was studied using PS latex NP coated with PS-*b*-PEG (PS block molecular weight of 1 and 1.5 kg/mol, and PEG block molecular weight of 3 kg/mol) using FNP [62]. Surface coverage was elucidated through dynamic light scattering analysis and the Baleux iodine complex assay to quantify PEG concentrations on latex spheres or in the micellar phase. Above a polymer concentration of 0.53 wt%, a distinct population of free micelles was observed along with coated PS spheres. The results reveal an increase in the original particle size from 246 nm without stabilizing polymer to plateau at 300 nm with increasing PS-*b*-PEG concentrations. The size increase is comparable to an added layer equivalent to the radius of a free micelle. PEG packing density analysis reveals a PEG surface coverage of 9.29 nm^2/polymer, which is less than the fully equilibrated chain of the same length (0.75 nm^2/polymer), and closer packed than the Flory size (13.6 nm^2/polymer).

M_W effects

The block copolymer properties affect the drug NP *in vivo* clearance behavior. The relationship between block copolymer structure and clearance is elucidated in a study using various amphiphilic diblock copolymers of PEG associated with a hydrophobic block of PS, PCL, PLA, or PLGA, of various molecular weights [63]. The NP clearance behavior of paclitaxel-VES conjugate NP *in vivo* stabilized using selected block copolymers, and the *in vitro* complement assay analysis, provided insight on the effect of polymer chemistry and M_w on NP circulation *in vivo*. The amount of paclitaxel-VES remaining in plasma four hours following injection of NP in mice was determined by HPLC and is shown in Fig. 7.

Reducing the PCL M_w while keeping the PEG M_w constant at 5000 g/mol increases protection, thanks to a more laterally compressed dense PEG layer. At constant PCL M_w, reducing the PEG M_w to 2000 g/mol provided less protection. These results suggest the relative anchoring area of the hydrophobic block compared with the solvated PEG chain, as well as the absolute PEG molecular weight affect the polymer stabilizing efficiency. Another effect identified through the study is the anchoring strength of the hydrophobic block relative to the solvation energy of the hydrophilic block. The hydrophobic block with the largest Log *P* value provided

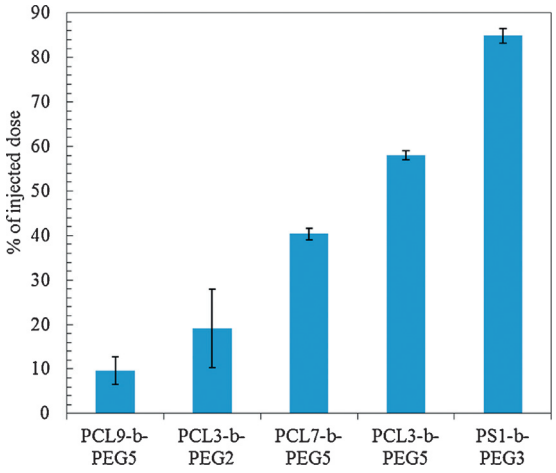

Figure 7 Paclitaxel-VES conjugate remaining in plasma four hours following injection in mice using NP stabilized with block copolymers of varying block lengths. Numbers subsequent to the block designation refer to the block molecular weight (kg/mol). Error bars represent standard deviation ($n = 3$). Figure adapted from [63].

better protection *in vivo*. Log *P* combines both the M_w effect and the hydrophobicity of the polymer. At the same M_w, PCL is an order of magnitude less hydrophobic than PS, which provided superior protection. Increasing the hydrophobicity of PCL through increasing its M_w makes it unfit for FNP due to kinetic limitations. The crystallinity of the hydrophobic block also affects its protection efficiency. As discussed earlier, stable formulations prepared by FNP require amorphous polymers. The *in vivo* results also reveal the poorest circulating NP were stabilized using PCL-*b*-PEG with the highest PCL M_w, which correlates with a higher tendency for crystallization.

In terms of particle stability, Zhu demonstrated that the hydrophobic block molecular weight does not affect particle size for PLGA-*b*-PEG NP of β-carotene prepared *via* FNP [58]. The study provides a guideline for block copolymer selection in NP formulation of hydrophobic drugs.

Other polymeric stabilizers

The use of polymer stabilizers in FNP is not restricted to block copolymers. For instance, Gelatin was adsorbed on polystyrene NP *via* FNP, and the stability of the resulting gelatin coated NP was investigated by *ex situ* dynamic light scattering as a function of mixing intensity. The results show a trend of increasing stability with increasing mixing intensity [64]. In another application, polyvinylpyrrolidone (PVP) and polyvinyl alcohol (PVOH) were used to produce stable NP of the pesticide bifenthrin using FNP [48].

Other examples of polymer stabilizers include polyelectrolytes. For instance, branched polyethyleneimine (PEI, M_w 750,000) was incorporated into NP *via* FNP using poly(acrylic acid)-*b*-poly(ethylene oxide) (PAA-*b*-PEO) [49]. Precipitation was induced through electrostatic interaction by mixing the block copolymer and PEI at equal charge in an MIVM. The resulting particle size was dependent on mixing until mixing was fast enough ($Re > 2000$) to provide homogenous

conditions. In another application, NP of β-carotene were successfully stabilized by steric and electrostatic effects using linear PEI, branched PEI, ε-polylysine (PL), or chitosan, with solute loadings up to 90 wt% [20]. The study results reveal enhanced NP stabilization using branched PEI compared with linear PEI, and with higher molecular weight polyelectrolytes.

More recently, non-polymers have been used in FNP for the production of curcumin NP *via* FNP [45]. Using the non-polymeric surfactants phosphatidylcholine and glycyrrhizinate salts, curcumin emulsions were processed *via* FNP to obtain stable, controlled size NP. The study demonstrates the use of a volatile oil-in-water emulsion as an alternative for the organic solution typically used in the FNP process.

Examples and applications

This section provides some examples of solutes formulated *via* FNP for various applications. Since its introduction in 2003, many solutes have been formulated into NP *via* FNP for various applications, as discussed in this review and summarized in Table 2.

Multiple actives NP

Recently, significant interest has been dedicated toward engineered nanomaterials with multifunctional capabilities, such as imaging, diagnostic and therapy, and multiple drug delivery [83]. Based on the previous discussion, it is now clear that FNP relies primarily on the condition of supersaturation followed by polymer arrested growth to yield controlled size solute NP. Therefore, co-precipitation of chemically different solutes is possible using FNP provided the condition of supersaturation is met for each precipitated component. The work of Gindy et al. illustrates this approach through co-precipitation into controlled size NP of colloidal gold (Au) as an illustrative imaging contrast agent and β-carotene as a model therapeutic [80]. Using FNP, inorganic Au colloids of about 5 nm in diameter were co-encapsulated with β-carotene as a model drug using PCL-*b*-PEG *via* FNP. The particle size was changed from 75 nm to 275 nm using PCL homopolymer. In another application pertaining to sunscreens, organic and inorganic UV filters were co-encapsulated using FNP to achieve broad-spectrum UVA, UVB, and UVC wavelength absorption [44]. Composite NP formulations were prepared using organic UV filters Uvinul A Plus, Uvinul T150, or Uvinul M 40, and the inorganic filters zinc oxide or titanium dioxide. Co-aggregation of T 150, A Plus, and titanium dioxide resulted in strong absorption over the UVA, UVB, and UVC wavelength. Additionally, particle size was tuned using PS as an inert co-solute, which allows for enhanced UV mitigation through both absorption and scattering.

Imaging

Formulating imaging agents into NP provides a formulation route for hydrophobic dyes, enhanced shielding from the biological environment, increased stability against oxidative degradation or photobleaching, and potentially increased brightness [84]. NP-based imaging contrast agents, particularly those based on iron oxide, gold, and semiconducting metals, provide improvements to imaging techniques such as X-ray, near-infrared fluorescence imaging, and magnetic resonance imaging [84]. Fig. 8 illustrates the use of long-wavelength fluorescent dyes for *in vivo* imaging.

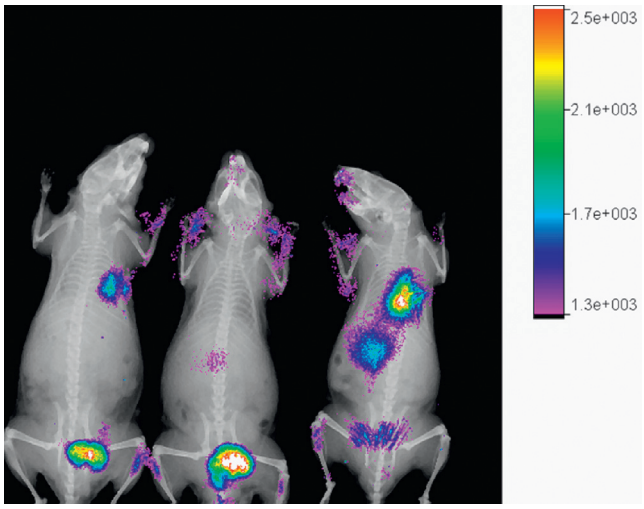

Figure 8 Long wavelength fluorescent dye NP used for *in vivo* imaging. Mice were injected with a 2 mg dose of the long wavelength dye particles through a 100 μL tail-vein injection, and were imaged 30 min post-dose. The center mouse is used as control. The two mice on the right and left are injected with fluorescent dye NP directed to the lungs.

One type of materials currently explored for bioimaging and photodynamic therapy applications are up-conversion phosphors (UCP) [78]. Using near-infrared light irradiation, UCP produce emissions in the visible spectrum, which addresses the limitation in tissue penetration observed with conventional down-converting imaging agents [85]. FNP was used to produce a stable composite NP system consisting of a UCP core, an intermediate coat of tetraphenylporphyrin, and a PEG layer allowing for oxygen penetration, singlet oxygen diffusion, and providing a biocompatible layer for enhanced *in vivo* circulation [78,85]. The NP dispersions formulated using PLGA-*b*-PEG or PLA-*b*-PEG were stable under physiological conditions. Particle size remained unchanged for seven days for samples in water, PBS buffer, or culture media. In contrast, the PCL crystallinity lead to instability in PCL-*b*-PEG stabilized NP [78].

FNP provides a platform for the preparation of multifunctional NP. Akbulut et al. use FNP for the preparation of fluorescent NP using nile red, coumarin, pyrene, anthracene, and porphyrin, and combinations of an organic solute (vitamin E) and a fluorophore in a single NP for simultaneous drug delivery and biological imaging [79]. NP were stabilized using PS-*b*-PEG, providing NP with emission peaks ranging from, but not limited to, 320 to 720 nm. More recently, FNP was used to produce high loading NP of a pentacene-based fluorescent dye with high hydrophobicity, photobleaching resistance, and a relatively long wavelength emission of 695 nm [74].

Table 2 Examples of NP formation *via* FNP.

Solute	Solute/study description	Stabilizer	Reference
Iron oxide-based nanocrystal and NIR dye tris-(porphyrinato)zinc(II)	MRI and fluorescent imaging agents	PLA-*b*-PEG	[65]
Hydrophobic aggregation-induced emission (AIE)-active dye of EDP	Fluorescent imaging agent	PCL-*b*-PEG	[66]
Curcumin	Many potentially beneficial therapeutic applications [67]	Phosphatidylcholine and glycyrrhizinate salts	[45]
		PLA-*b*-PEG	[68,69]
None	Study illustrates the use of Zein, a corn product, in FNP	Zein	[70]
Rifampicin, antibiotic SQ641, cyclosporine A	Tuberculosis treatment	PLGA-*b*-PEG	[71]
Tannic acid	Antioxidant	PS-*b*-PEG	[72]
Au or Pt	Hybrid metal nanoparticle deposited onto spherical polymer assemblies	PS-*b*-PVP	[73]
Et-TP5	Formation of fluorescent dye NP of a pentacene derivative dye for biomedical imaging	PS-*b*-PEG	[74]
β-Carotene, hydrocortisone, betulin, paclitaxel	NP stability enhancement using chemical conjugation, and correlation with Log *P* of drug molecules	PLGA-*b*-PEG	[18]
CdSe core-only and CdSe—ZnS core—shell nanocrystals	Formation of stable quantum dots NP.	PS-*b*-PEG; Pluronic F127	[75]
β-Carotene, hydrocortisone, betulin, paclitaxel, triiodophenol	Effect of BCP, solute, and formulation conditions on the formation and stability of NP.	PS-*b*-PEG; PCL-*b*-PEG, PLA-*b*-PEG, PLGA-*b*-PEG	[56—58]
Progesterone	NP formation of a promising therapeutic for treating traumatic brain injury	PLA-*b*-PEG	[42]
SR13668	NP formation of an anti-cancer drug candidate with limited bioavailability.	PLGA	[43]
Ethylhexyl triazone (Uvinul T 150), benzophenone-3 (Uvinul M 40), diethylamino hydroxybenzoyl hexyl benzoate (Uvinul A Plus), zinc oxide, and titanium dioxide	Inorganic and organic hydrophobic sunscreen filters incorporation into NP	PS-*b*-PEG	[44]
Bioactive amphiphilic macromolecule (AM)	NP containing AM, a potential active for counteracting atherosclerotic plaque development	PLA-*b*-*PEG*	[76]
β-Carotene and PEI	NP formation of a model hydrophobic drug and a macromolecule.	PS-*b*-PEG; PCL-*b*-PEG, PAA-*b*-PEO	[49]
Upconverting nanophosphors (UCNP) and meso-tetraphenyl porphyrin (TPP)	NP formation of UCNP and TPP for photodynamic therapy and bioimaging.	PLA-*b*-PEG	[77]
Upconverting nanophosphors (UCNP)	NP formation of UCNP with enhanced stability in DI water, PBS buffer, or culture media.	PLC-*b*-PEG; PLA-*b*-PEG, PLGA-*b*-PEG	[78]
β-Carotene	NP formation using polyelectrolytes.	Linear/branched PEI, chitosan, PL	[20]

Table 2 (*Continued*)

Solute	Solute/study description	Stabilizer	Reference
Pyrene and vitamin E	Formation of multifunctional fluorescent NP for simultaneous drug delivery and biological imaging.	PCL-*b*-PEG; Functional PCL-*b*-PEG	[79]
Bifenthrin	NP formation of bifenthrin, a model pesticide.	PCL-*b*-PEG; PS-*b*-PEG; pluronic F127; PVOH; PVP; poly(acrylic acid)-*b*-poly(butyl acrylate)	[48]
β-Carotene and Au	Simultaneous encapsulation of organic actives and inorganic nanostructures	PCL-*b*-PEG	[80]
Clarithromycin	NP formation of a macrolide antibiotic.	Carboxylmethyl cellulose acetate butyrate	[81]
Paclitaxel	NP formation of paclitaxel prodrugs resulting in enhanced efficacy *in vivo*.	PS-*b*-PEG	[50]
β-Carotene	NP formation of a hydrophobic solute.	PS-*b*-PEG	[82]

Targeting

In addition to exploiting passive targeting through the EPR effect, functionalizing NP surfaces by tumor-specific ligands provides opportunities for active targeting of cell surface receptors that triggers NP internalization into the cell. FNP provides a platform for the development of NP carriers with targeting capabilities. One application uses NP functionalized with the Luteinizing Hormone-Releasing Hormone (LHRH) targeting peptide, resulting in enhanced *in vitro* cellular uptake [79]. Fig. 9 demonstrates uptake of 80 nm PEG-protected NP into MS578T breast cancer cells with LHRH targeting.

The versatility and ease of preparation of such formulations was illustrated using bovine serum albumin (BSA) as a model ligand for the formation of BSA bioconjugated NP with accurate control of ligand density [86]. The study uses reactive block copolymers of PCL-*b*-PEG with PEG terminated maleimide functionality, which provide reactive sites for subsequent conjugation. The surface density of PCL-*b*-PEG-maleimide is simply controlled by the fraction of reactive block copolymers used in the inlet stream of the MIVM mixer. NP formation is followed by surface conjugation with BSA *via* thiol-maleimide reaction, with up to 22% PEG-maleimide tethers reaction. Another study demonstrates the use of FNP to produce and optimize NP with targeting ligands for tuberculosis drug delivery [87]. The NP surface was functionalized with mannoside moieties that bind to the mannose receptor, a transmembrane protein that binds to mannose caps on the mycobacterium tuberculosis. Binding and uptake were evaluated *in vitro* using the murine macrophage J774 cell line. The study reveals the effect of several factors on the binding and internalization of targeted NP, including the terminal groups on PEG covering the NP surface, NP size, and ligand density. Using methoxy-terminated PEG chains passivates the NP surface and evades recognition irrespective of particle size, while using hydroxyl-terminated PEG chains shows a size-dependent association, whereby larger particles provide increased association. Mannoside functionalization of PEG chain ends provides a threefold increase in binding compared with non-targeted NP independent of PEG molecular weight. A maximum was observed at a ligand density of 9%, beyond which binding decreases. The study illustrates the flexibility of FNP as a simple method for developing and optimizing novel drug NP formulations with active targeting functionalities.

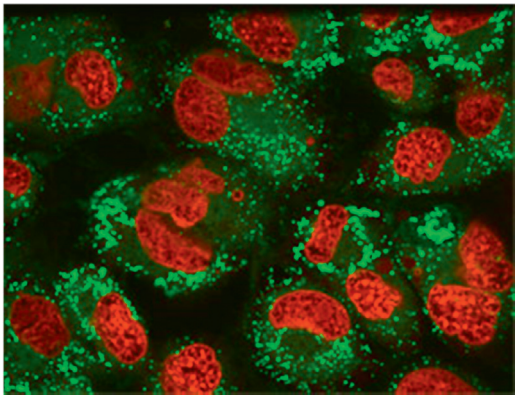

Figure 9 MS578T breast cancer cellular uptake of LHRH PEG-protected NP containing Nile Red fluorescent dye. The red areas are Draq-5 stained cell nuclei.

In another application focusing on atherosclerotic plaque development, FNP was used to formulate bioactive amphiphilic macromolecules (AM) into NP with enhanced stability and cell-targeted biological efficacy [76]. AM are being explored as therapeutic ligands for inflammatory cells with increased inhibition of atherosclerosis. Unlike

kinetically assembled NP, micelle-based assemblies of AM limit their efficacy due to micellar integrity limitations under physiological conditions. NP formulations were prepared using bioactive AM composed of PEG conjugated to mucic acid modified with lauroyl groups, and either a carboxylic acid or propyl amide terminal functionality. PLA or mucic acid modified with lauroyl groups were mixed with AM to provide hydrophobic core anchoring sites with high affinity to the AM hydrophobic domains. Under physiologically relevant conditions, the resulting formulations reveal colloidal stability and biological activity, shown through the degree of inhibition of oxidized low-density lipoprotein uptake in inflammatory cells consisting of human monocyte-derived macrophages. The resulting NP demonstrate enhanced efficacy compared with micellar formulations, and show affinity toward cell surface receptors involved in atherosclerotic lesions development.

Process of optimization

One example illustrating the optimization of solute NP formation using FNP is the formulation of high-loading progesterone NP [42]. Progesterone is a neurosteroid with promising therapeutic potential for traumatic brain injury (TBI). It exhibits high hydrophobicity and high crystallinity, which limits its administration at therapeutically relevant doses. FNP processing of progesterone with PLA-*b*-PEG yielded a cloudy solution with large aggregates due to the relatively low supersaturation (progesterone solubility in 10% THF is 0.42 mg/mL) achieved through mixing. However, addition of D-α-tocopherol (TOC) as a nucleating agent and solubilizer for progesterone resulted in stable NP formation with drug loading of about 24% and encapsulation efficiency of 69.4% and a final progesterone concentration of 10.8 ± 0.2 mg/mL. Particle size distribution was monomodal with an average of 270 nm. TOC preferentially partitions into a polymeric shell instead of phase separating into the aqueous media, and provides a sink for progesterone. The study demonstrates the production of high concentration progesterone NP formulations with high drug loadings using FDA-approved GRAS components.

Post processing

Solvent removal requirement

The FNP process yields solute NP dispersions in aqueous and organic solvent mixtures. The high interfacial area between the solute NP and surrounding liquid leads to instabilities, including particle aggregation, recrystallization, and Ostwald ripening, which requires post processing of the NP formulations to ensure stability. One study investigated the Ostwald ripening of β-carotene NP produced by FNP and stabilized using PS-*b*-PEO at varying organic solvent content [10]. The Lifshitz, Slyozov, and Wagner theory for particle growth was numerically implemented to predict diffusion-mediated particle growth, and revealed quantitative agreement with experimental results. The study shows that the most effective means of reducing particle growth through Ostwald ripening is reduction of solute solubility, which is achieved by removing residual solvent introduced through the FNP process. A subsequent study using itraconazole and odanacatib formulations prepared by FNP provides further information on factors affecting NP stability [59]. The time scale for diffusion-controlled growth kinetics, t_d is given by [59]

$$t_d = \frac{RT\, r_3}{\gamma v^2 D C_{eq}} \tag{7}$$

Where R is the gas constant, r the particle size, D is the diffusion coefficient, and C_{eq} is the equilibrium solubility. The scaling suggested by the time scale expression and the experimental results reveal that in addition to the equilibrium solubility, temperature, particle size, and molar volume affect the ripening rate. Reducing the storage temperature and removing residual organic solvent enhances the formulation stability profile. Additionally, drug product residual solvent content should be limited in pharmaceutical applications based on the solvent classification and permitted daily exposure [88]. Methods for removing solvents from NP dispersions are briefly discussed in the next sections.

Dialysis

One method for the removal of organic solvent following NP formation by FNP is dialysis. This technique uses a dialysis membrane with specific molecular weight cutoff that allows for solvent exchange but prevents larger particle diffusion. NP dispersions are placed in a dialysis bag and exchanged against a batch of water, which is replaced several times over roughly 24 h, resulting in reduction of the amount of organic solvent. Care should be taken in selecting the dialysis bag materials of construction to ensure proper membrane resistance to the solvent used. While this method is convenient at the bench scale, it is time consuming for industrial scale applications. Additionally, depending on the formulated solute, the processing time scale involved in dialysis might be sufficient for solvent mediated instabilities to occur. To overcome this limitation, crossflow microfiltration can be used to remove solvent and other residual impurities such as excess ligands, monomers, or stabilizers. In this technique, efficiency is enhanced by continuous exchange of the NP dispersion with water across a membrane with a specific area and molecular weight cutoff. In one application, a two liter feed is processed in 2.5 h through crossflow microfiltration in a concentration step followed by a diafiltration step [89].

Flash evaporation

Typical solvents used in FNP such as THF have lower boiling points than water, and can be conveniently removed by evaporation under reduced pressure conditions [90]. In flash evaporation, liquid effluent product from the FNP mixer is preheated and subjected to reduced pressure that induces partial vaporization, resulting in organic solvent removal [91]. Using β-carotene as model hydrophobic solute, NP suspensions prepared with THF as the organic solvent were preheated to 45 °C, and fed to a vacuum chamber twice. The process reduced residual solvent concentration to levels acceptable for drug applications, with

96% solvent removal after two-stage flash evaporation, in agreement with phase equilibria calculations. The success of this method was partially attributed to the non-ideality in the vapor—liquid equilibrium of the water—THF mixture, which favors solvent removal. Flash evaporation is suited for volatile organic solvents that do not exhibit azeotropes with water.

Freeze drying

Alternatively, freeze drying or lyophilization can be used for complete removal of both water and organic solvent from NP dispersions, resulting in dry powder solids with prolonged chemical and physical stability [92]. Lyophilization is typically conducted in three phases under controlled temperature and pressure conditions: first, the NP dispersion is solidified by freezing below the glass transition temperature for amorphous formulations or the eutectic temperature for crystalline formulations, followed by ice sublimation, and finally secondary drying to achieve desorption of unfrozen water [92]. The freeze drying process is an expensive unit operation in pharmaceutical manufacturing that involves several tunable parameters, including temperature, heating/freezing rates, and cryoprotectant type and concentrations [92]. Simply drying NP dispersions by rotary evaporation causes irreversible aggregation and the formation of aggregates larger than 1 μm, while freeze drying requires addition of significant amounts of cryoprotectant to minimize aggregation upon NP redispersion [43,93]. For instance, to minimize aggregation, β-carotene NP dispersions produced by FNP and stabilized with PLGA-*b*-PEG were freeze dried using sucrose as a cryoprotectant at a NP/sucrose weight ratio of 1/60 [93]. The large amounts of cryoprotectant needed present limitations to the NP concentration that can be administered *in vivo* while maintaining isotonic conditions. Alternative excipients have been identified for optimal cryoprotection. For instance, nitric oxide prodrug NP produced by FNP were freeze dried using trehalose and Pluronic F68 at a NP/cryoprotectant weight ratio of 1/18.5 [94]. In the case of progesterone formulated with TOC, freeze drying using Pluronic F68 as a cryoprotectant at a NP/Pluronic weight ratio of 3/4 yielded stable dry powders that can be reconstituted at clinically relevant concentrations and osmolarity by simple hand agitation, while maintaining original particle size [42].

Alternatively, concentrating and drying NP can be achieved through hydrogen bonding coacervate precipitation (HBCP) [93]. HBCP is a fast process that exploits hydrogen bonding interactions between PEG on the NP surface and polycarboxylic acid compounds to reversibly precipitate NP suspensions, while avoiding sample exposure to thermal stress. Addition of the acid to the NP suspension following FNP leads to a fast, reversible precipitation of a coacervate, induced by hydrogen bonding of the acid and the PEG chains. The coacervate is recovered by centrifugation or filtration, which removes most of the liquid, and dried by conventional drying or freeze drying. Recovery of the NP suspension is achieved by ionization of the acid groups to pH > 7, which breaks hydrogen bonding and causes complex dissociation and resuspension of the NP to within 10% of their original size.

Spray drying and spray freeze drying

Solvent removal can also be achieved through spray drying. In one application involving the formation of porous NP aggregate particles (PNAP) for drug delivery to the lung, the MIVM was integrated to a spray dryer to allow for NP formation and drying in one step [95]. Using this setup, a drug conjugate of the antibiotic rifampicin was formulated into NP *via* FNP and spray dried with the amino acid leucine from an ethanol/water solution to yield PNAP. The resulting particle size and structure were suitable for deep lung deposition.

Spray freeze drying involves atomization of the NP suspension in a cryogenic liquid to induce fast freezing followed by the lyophilization drying steps [96]. This method has been used with FNP to produce NP embedded micron sized particles for therapeutics delivery by aerosol inhalation [97]. Delivery of NP to the lungs is attractive because NP in the 100—200 nm size range are retained in the lung longer than micron-sized particles. However, in the ~100 nm size range, particle delivery to the lung surface as a powder aerosol is difficult [98]. One approach to resolve this is to embed NP in a soluble matrix to form micron sized particles, which can be delivered to the lung surface as a powder aerosol. The larger particles dissociate quickly to yield NP deposited on the lung surface. Using FNP, cholesterol NP were spray freeze dried in a mannitol matrix using ultrasonic atomization. The resulting powders increased in size upon redispersion, but yielded particle sizes <250 nm upon sonication. In contrast, spray drying resulted in irreversible aggregation and low powder yields.

Conclusions

The factors controlling NP formation by FNP have been elucidated. The current understanding of particle formation by rapid precipitation and subsequent stabilization makes FNP a platform technology that can be exploited for several applications thanks to high loading efficiencies, loading contents, control of particle size, and flexibility in incorporating multiple actives. The starting point in FNP is imposing uniform high supersaturation conditions that affect nucleation and growth rates. This is achieved by fast mixing through various geometries (CIJ, MIVM), leading to simultaneous incorporation of multiple species, and block copolymer arrested particle growth. Conjugation, ion pairing, and the use of co-solutes provide NP formulation opportunities for a wide range of actives, while the production of multifunctional NP expands the scope of applications where FNP can be beneficial. The method is easily scalable and the post processing of formulations produced by FNP ensures particle stability. The range of applications for FNP is bound to grow as the understanding of the process mechanism is further elucidated.

Acknowledgements

The authors thank Mr. Emilio El Zir for assistance with the graphical abstract design. W.S. acknowledges support from

the American University of Beirut's junior faculty research leave program.

References

[1] C. Clavero, Nat. Photonics 8 (2014) 95.
[2] M. Klapper, C.G. Clark, K. Muellen Jr., Polym. Int. 57 (2008) 181.
[3] K.M. Gharpure, S.Y. Wu, C. Li, G. Lopez-Berestein, A.K. Sood, Clin. Cancer Res. 21 (2015) 3121.
[4] A. Dickherber, S.A. Morris, P. Grodzinski, Wiley Interdiscip. Rev. Nanobiotechnol. 7 (2015) 251.
[5] M. Morgen, C. Bloom, R. Beyerinck, A. Bello, W. Song, K. Wilkinson, et al., Pharm. Res. 29 (2012) 427.
[6] D. Peer, J.M. Karp, S. Hong, O.C. Farokhzad, R. Margalit, R. Langer, Nat. Nanotechnol. 2 (2007) 751.
[7] N. El-Gendy, M.M. Bailey, C. Berkland, in: H.D.C. Smyth, A.J. Hickey (Eds.), Controlled Pulmonary Drug Delivery, Springer, New York, 2011, pp. 283—312.
[8] V.C.F. Mosqueira, P. Legrand, J.L. Morgat, M. Vert, E. Mysiakine, R. Gref, et al., Pharm. Res. 18 (2001) 1411.
[9] S. Svenson, Curr. Opin. Solid State Mater. Sci. 16 (2012) 287.
[10] Y. Liu, K. Kathan, W. Saad, R.K. Prud'homme, Phys. Rev. Lett. 98 (2007) 036102.
[11] V. Kumar, R.K. Prud'homme, J. Pharm. Sci. 97 (2008) 4904.
[12] B.K. Johnson, W. Saad, R.K. Prud'homme, in: S. Svenson (Ed.), Polym. Drug Deliv. II Polym. Matrices and Drug Part. Eng., American Chemical Society, Washington, DC, USA, 2006, pp. 278—291.
[13] S. Kim, B. Lotz, M. Lindrud, K. Girard, T. Moore, K. Nagarajan, et al., Org. Process Res. Dev. 9 (2005) 894.
[14] D. Horn, J. Rieger, Angew. Chem. Int. Ed. 40 (2001) 4330.
[15] B.K. Johnson, R.K. Prud'homme, AIChE J. 49 (2003) 2264.
[16] S.M. D'Addio, R.K. Prud'homme, Adv. Drug Deliv. Rev. 63 (2011) 417.
[17] A.J. Mahajan, D.J. Kirwan, J. Cryst. Growth 144 (1994) 281.
[18] Z. Zhu, Mol. Pharm. 11 (2014) 776.
[19] K. Letchford, R. Liggins, H. Burt, J. Pharm. Sci. 97 (2008) 1179.
[20] Z. Zhu, K. Margulis-Goshen, S. Magdassi, Y. Talmon, C.W. Macosko, J. Pharm. Sci. 99 (2010) 4295.
[21] Dormidontova, Macromolecule 32 (1999) 7630.
[22] C. Ligoure, L. Leibler, J. Phys. Fr. 51 (1990) 1313.
[23] B. Johnson, R. Prud'homme, Phys. Rev. Lett. 91 (2003) 118302.
[24] J. Baldyga, J.R. Bourne, Chem. Eng. J. 42 (1989) 83.
[25] J. Bałdyga, R. Pohorecki, Chem. Eng. J. 58 (1995) 183.
[26] M. Barrett, D. O'Grady, E. Casey, B. Glennon, Chem. Eng. Sci. 66 (2011) 2523.
[27] J. Han, Z. Zhu, H. Qian, A.R. Wohl, C.J. Beaman, T.R. Hoye, et al., J. Pharm. Sci. 101 (2012) 4018.
[28] J. Baldyga, W. Podgorska, R. Pohorecki, Chem. Eng. Sci. 50 (1995) 1281.
[29] M.C. Fournier, L. Falk, J. Villermaux, Chem. Eng. Sci. 51 (1996) 5053.
[30] Y. Shi, J.C. Cheng, R.O. Fox, M.G. Olsen, J. Micromech. Microeng. 23 (2013) 1.
[31] J.C. Cheng, M.G. Olsen, R.O. Fox, Appl. Phys. Lett. 94 (2009) 204104.
[32] Y. Liu, R.O. Fox, AIChE J. 52 (2006) 731.
[33] Y. Liu, C. Cheng, Y. Liu, R.K. Prud'homme, R.O. Fox, Chem. Eng. Sci. 63 (2008) 2829.
[34] E. Gavi, D.L. Marchisio, A.A. Barresi, Chem. Eng. Sci. 62 (2007) 2228.
[35] D.L. Marchisio, Comput. Chem. Eng. 33 (2009) 408.
[36] N. Di Pasquale, D.L. Marchisio, A.A. Barresi, Chem. Eng. Sci. 84 (2012) 671.
[37] N. Di Pasquale, D.L. Marchisio, P. Carbone, A.A. Barresi, Chem. Eng. Res. Des. 91 (2013) 2275.
[38] W.L. Jorgensen, E.M. Duffy, Adv. Drug Deliv. Rev. 54 (2002) 355.
[39] A. Tiwari, A. Tiwari, Nanomaterials in Drug Delivery, Imaging, and Tissue Engineering, John Wiley & Sons, Somerset, NJ, USA, 2013.
[40] E.S. Souza, L. Zaramello, C.A. Kuhnen, B.d.S. Junkes, R.A. Yunes, V.E. Fonseca Heinzen, Int. J. Mol. Sci. 12 (2011) 7250.
[41] CRC Handbook of Chemistry and Physics, 90th ed., CRC Press, Boca Raton, FL, USA, 2009—2010.
[42] C.E. Figueroa, P. Reider, P. Burckel, A.A. Pinkerton, R.K. Prud'homme, Ther. Deliv. 3 (2012) 1269.
[43] H. Shen, A.A. Banerjee, P. Mlynarska, M. Hautman, S. Hong, I.M. Kapetanovic, et al., J. Pharm. Sci. 101 (2012) 3877.
[44] L. Shi, J. Shan, Y. Ju, P. Aikens, R.K. Prud'homme, Colloids Surf. A: Physicochem. Eng. Aspects 396 (2012) 122.
[45] K. Margulis, S. Magdassi, H.S. Lee, C.W. Macosko, J. Colloid Interface Sci. 434 (2014) 65.
[46] M.E. Gindy, K. DiFelice, V. Kumar, R.K. Prud'homme, R. Celano, R.M. Haas, et al., Langmuir 30 (2014) 4613.
[47] T. Chen, S.M. D'Addio, M.T. Kennedy, A. Swietlow, I.G. Kevrekidis, A.Z. Panagiotopoulos, et al., Nano Lett. 9 (2009) 2218.
[48] Y. Liu, Z. Tong, R.K. Prud'homme, Pest Manag. Sci. 64 (2008) 808.
[49] H. Shen, S. Hong, R.K. Prud'homme, Y. Liu, J. Nanopart. Res. 13 (2011) 4109.
[50] S.M. Ansell, S.A. Johnstone, P.G. Tardi, L. Lo, S. Xie, Y. Shu, et al., J. Med. Chem. 51 (2008) 3288.
[51] A.R. Wohl, A.R. Michel, S. Kalscheuer, C.W. Macosko, J. Panyam, T.R. Hoye, J. Med. Chem. 57 (2014) 2368.
[52] N.M. Pinkerton, A. Grandeury, A. Fisch, J. Brozio, B.U. Riebesehl, R.K. Prud'homme, Mol. Pharm. 10 (2013) 319.
[53] M.E. Gindy, A.M. Leone, J.J. Cunningham, Expert Opin. Drug Deliv. 9 (2012) 171.
[54] M.E. Gindy, B. Feuston, A. Glass, L. Arrington, R.M. Haas, J. Schariter, et al., Mol. Pharm. 11 (2014) 4143.
[55] S.M. Moghimi, A.C. Hunter, J.C. Murray, Pharmacol. Rev. 53 (2001) 283.
[56] Z. Zhu, Polymer Stabilized Nanosuspensions Formed via Flash Nanoprecipitation: Nanoparticle Formation, Formulation, and Stability (Ph.D. thesis), University of Minnesota, 2010.
[57] K.M. Pustulka, A.R. Wohl, H.S. Lee, A.R. Michel, J. Han, T.R. Hoye, et al., Mol. Pharm. 10 (2013) 4367.
[58] Z. Zhu, Biomaterials 34 (2013) 10238.
[59] V. Kumar, L. Wang, M. Riebe, H.-H. Tung, R.K. Prud'homme, Mol. Pharm. 6 (2009) 1118.
[60] Z. Zhu, J.L. Anacker, S. Ji, T.R. Hoye, C.W. Macosko, R.K. Prud'homme, Langmuir 23 (2007) 10499.
[61] M.E. Matteucci, M.A. Hotze, K.P. Johnston, R.O. Williams III, Langmuir 22 (2006) 8951.
[62] S.J. Budijono, B. Russ, W. Saad, D.H. Adamson, R.K. Prud'homme, Colloids Surf. A: Physicochem. Eng. Aspects 360 (2010) 105.
[63] S.M. D'Addio, W. Saad, S.M. Ansell, J.J. Squiers, D.H. Adamson, M. Herrera-Alonso, et al., J. Control. Release 162 (2012) 208.
[64] M. Akbulut, N.K. Reddy, B. Bechtloff, S. Koltzenburg, J. Vermant, R.K. Prud'homme, Langmuir 24 (2008) 9636.
[65] N.M. Pinkerton, M.E. Gindy, V.L. Calero-DdelC, T. Wolfson, R.F. Pagels, D. Adler, et al., Adv. Healthc. Mater. 4 (2015) 1376.
[66] M.W. Wang, N. Yang, Z.Q. Guo, K.Z. Gu, A.D. Shao, W.H. Zhu, et al., Ind. Eng. Chem. Res. 54 (2015) 4683.
[67] M.M. Yallapu, P.K.B. Nagesh, M. Jaggi, S.C. Chauhan, AAPS J. 17 (2015) 1341.
[68] S.F. Chow, C.C. Sun, A.H.L. Chow, Eur. J. Pharm. Biopharm. 88 (2014) 462.
[69] S.F. Chow, K.Y. Wan, K.K. Cheng, K.W. Wong, C.C. Sun, L. Baum, et al., Eur. J. Pharm. Biopharm. 94 (2015) 436.
[70] K. Li, X. Zhang, Q. Huang, S. Yin, X. Yang, Q. Wen, et al., J. Food Eng. 127 (2014) 103.

[71] S.M. D'Addio, V.M. Reddy, Y. Liu, P.J. Sinko, L. Einck, R.K. Prud'homme, Mol. Pharm. 12 (2015) 1554.
[72] C. Tang, D. Amin, P.B. Messersmith, J.E. Anthony, R.K. Prud'homme, Langmuir 31 (2015) 3612.
[73] R. Liu, C. Sosa, Y.-W. Yeh, F. Qu, N. Yao, R.K. Prud'homme, et al., J. Mater. Chem. A 2 (2014) 17286.
[74] V.J. Pansare, M.J. Bruzek, D.H. Adamson, J. Anthony, R.K. Prud'homme, Mol. Imaging Biol. 16 (2014) 180.
[75] Y. Zhang, A.R. Clapp, RSC Adv. 4 (2014) 48399.
[76] A.W. York, K.R. Zablocki, D.R. Lewis, L. Gu, K.E. Uhrich, R.K. Prud'homme, et al., Adv. Mater. 24 (2012) 733.
[77] J. Shan, S.J. Budijono, G. Hu, N. Yao, Y. Kang, Y. Ju, et al., Adv. Funct. Mater. 21 (2011) 2488.
[78] S.J. Budijono, J. Shan, N. Yao, Y. Miura, T. Hoye, R.H. Austin, et al., Chem. Mater. 22 (2010) 311.
[79] M. Akbulut, P. Ginart, M.E. Gindy, C. Theriault, K.H. Chin, W. Soboyejo, et al., Adv. Funct. Mater. 19 (2009) 718.
[80] M.E. Gindy, A.Z. Panagiotopoulos, R.K. Prud'homme, Langmuir 24 (2008) 83.
[81] J.M. Pereira, R. Mejia-Ariza, G.A. Ilevbare, H.E. McGettigan, N. Sriranganathan, L.S. Taylor, et al., Mol. Pharm. 10 (2013) 4640.
[82] B.K. Johnson, R.K. Prud'homme, Aust. J. Chem. 56 (2003) 1021.
[83] M.E. Gindy, R.K. Prud'homme, Expert Opin. Drug Deliv. 6 (2009) 865.
[84] V.J. Pansare, S. Hejazi, W.J. Faenza, R.K. Prud'homme, Chem. Mater. 24 (2012) 812.
[85] B. Ungun, R.K. Prud'homme, S.J. Budijono, J. Shan, S.F. Lim, Y. Ju, et al., Opt. Express 17 (2009) 80.
[86] M.E. Gindy, S. Ji, T.R. Hoye, A.Z. Panagiotopoulos, R.K. Prud'homme, Biomacromolecules 9 (2008) 2705.
[87] S.M. D'Addio, S. Baldassano, L. Shi, L. Cheung, D.H. Adamson, M. Bruzek, et al., J. Control. Release 168 (2013) 41.
[88] D. Jacobson-Kram, T. McGovern, Adv. Drug Deliv. Rev. 59 (2007) 38.
[89] I. Limayem, C. Charcosset, H. Fessi, Sep. Purif. Technol. 38 (2004) 1.
[90] E. Lepeltier, C. Bourgaux, P. Couvreur, Adv. Drug Deliv. Rev. 71 (2014) 86.
[91] V. Kumar, R.K. Prud'homme, Chem. Eng. Sci. 64 (2009) 1358.
[92] W. Abdelwahed, G. Degobert, S. Stainmesse, H. Fessi, Adv. Drug Deliv. Rev. 58 (2006) 1688.
[93] S.M. D'Addio, C. Kafka, M. Akbulut, P. Beattie, W. Saad, M. Herrera, et al., Mol. Pharm. 7 (2010) 557.
[94] V. Kumar, S.Y. Hong, A.E. Maciag, J.E. Saavedra, D.H. Adamson, R.K. Prud'homme, et al., Mol. Pharm. 7 (2010) 291.
[95] Y. Liu, Formulating Nanoparticles by Flash Nanoprecipitation for Drug Delivery and Sustained Release (Ph.D. thesis), Princeton University, 2007.
[96] S.M. D'Addio, J.G.Y. Chan, P.C.L. Kwok, R.K. Prud'homme, H.-K. Chan, Int. J. Pharm. 427 (2012) 185.
[97] S.M. D'Addio, J.G.Y. Chan, P.C.L. Kwok, B.R. Benson, R.K. Prud'homme, H.-K. Chan, Pharm. Res. 30 (2013) 2891.
[98] H. Chiou, H.-K. Chan, D. Heng, R.K. Prud'homme, J.A. Raper, J. Aerosol Sci. 39 (2008) 500.

Walid S. Saad is an assistant professor of chemical engineering at the American University of Beirut (AUB). Since joining AUB in the fall of 2010, Walid's research interests have been mostly focused on nanotechnology for drug delivery and the management of pharmaceuticals in the environment. Prior to joining AUB, Walid assumed the position of senior scientist at Merck (formerly Schering-Plough), New Jersey, USA. For about four years, he worked on the development of parenteral formulations for drug candidates in the oncology area. Prior to his involvement in the pharmaceutical industry, Walid obtained his PhD in chemical engineering working with Prof. Robert Prud'homme at Princeton University, New Jersey, USA. His graduate work focused on the design of novel polymer-based nanoparticle formulations for the controlled delivery of active agents. Walid holds a B.S. in chemical engineering from the University of Minnesota, and a B.S. in chemistry from the Lebanese American University in Beirut.

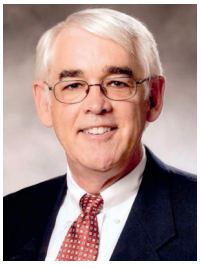

Robert K. Prud'homme is a professor in the Department of Chemical and Biological Engineering and Director of the Engineering Biology Program at Princeton University. He received his BS at Stanford University and his PhD from the University of Wisconsin at Madison under Professor Bob Bird. He has served on the executive committees of the American Institute of Chemical Engineers Materials Science Division and the U.S. Society of Rheology for which he served as President. He was the chair of the Technical Advisory Board for Material Science Research for Dow Chemical Company, and he was on the Board of Directors of Rheometric Scientific Inc. He also served on the Nanotechnology Scientific Advisory Committee for BASF. He directed the Princeton-University of Minnesota-Iowa State NSF NIRT Center on nanoparticle formation. His research interests include rheology and self-assembly of complex fluids with applications in nanoparticle formation for drug delivery, controlled release, targeting, and imaging.